atmosphere

MDPI

Article

The Impact of Stratospheric Intrusion on Surface Ozone in Urban Areas of the Northeastern Tibetan Plateau

Mingge Li, Yawen Kong, Meng Fan, Chao Yu, Ying Zhang, Jianbin Gu, Jinhua Tao * and Liangfu Chen

State Key Laboratory of Remote Sensing and Digital Earth, Aerospace Information Research Institute, Chinese Academy of Sciences, Beijing 100101, China
* Correspondence: taojh@aircas.ac.cn

Abstract: In recent years, high-altitude cities with low emissions in western China have exhibited an upward trend in surface ozone (O_3). Based on observations and reanalysis data, this study analyzed the evolutionary characteristics and pollution mechanisms of ozone in Xining and quantified the impact of stratospheric intrusion. The results indicated that an upward trend in summer O_3 was observed in Xining. A total of 29 ozone exceedance days were found. Potential exceedance days (>150 and >140 μg/m^3) showed substantial increases from 2022 to 2023. Using a stratospheric intrusion to surface (SITS) event identification algorithm, 42 events were found in Xining, with an average duration of 8.4 h. Spring exhibited the highest event frequency (13 events) and longest average duration. SITS events contributed an average of 19.7% to surface ozone, significantly exacerbating local exceedance risks. A typical ozone pollution episode from 25 July to 3 August 2021 was analyzed. The peak O_3 reached 170 μg/m^3. Elevated temperature, intensified radiation, and unfavorable meteorological conditions synergistically promoted local photochemical ozone production and accumulation. Notably, a SITS event was simultaneously detected, elevating surface ozone by 24%, which confirmed that stratospheric intrusion was the main cause of pollution.

Keywords: ozone; air pollution; Qinghai–Tibet Plateau; stratospheric intrusion

check for updates

Academic Editor: Hui Zhao

Received: 15 May 2025
Revised: 7 June 2025
Accepted: 10 June 2025
Published: 12 June 2025

Citation: Li, M.; Kong, Y.; Fan, M.; Yu, C.; Zhang, Y.; Gu, J.; Tao, J.; Chen, L. The Impact of Stratospheric Intrusion on Surface Ozone in Urban Areas of the Northeastern Tibetan Plateau. *Atmosphere* **2025**, *16*, 708. https://doi.org/10.3390/atmos16060708

Copyright: © 2025 by the authors. Licensee MDPI, Basel, Switzerland. This article is an open access article distributed under the terms and conditions of the Creative Commons Attribution (CC BY) license (https://creativecommons.org/licenses/by/4.0/).

1. Introduction

Surface ozone is primarily generated through photochemical reactions involving volatile organic compounds (VOCs) and nitrogen oxides (NOx). As a secondary pollutant, ozone pollution exerts substantial ecological impacts. Elevated ozone concentrations pose significant threats to both public health and ecosystems, including vegetation suppression, agricultural yield depression, and material degradation [1,2]. Furthermore, as a greenhouse component, ozone influences global climate change by altering radiative forcing in the Earth–atmosphere system [3–5]. In addition to precursor emissions, meteorological conditions represent a significant factor influencing ozone concentrations. For instance, high temperatures can increase emissions of NOx and VOCs and promote ozone formation [6–8], while surface solar radiation enhances ozone levels by altering the photochemical reaction rates of ozone production [9–12]. Some studies have also demonstrated that relative humidity (RH) serves as another crucial parameter governing ozone formation [13,14]. Adverse synoptic patterns inhibit pollutant dispersion, leading to pollutant accumulation [15]. Moreover, meteorologically driven transport processes significantly influence ozone pollution. Horizontal transport can increase ozone and precursor concentrations downwind of source regions [16–18]. Anomalous stratosphere–troposphere exchange (STE)

is often associated with synoptic-scale weather systems. Processes such as tropopause folding within extratropical cyclones, cut-off lows, and the outflow of deep convection could facilitate the downward transport of ozone-rich upper air masses, elevating tropospheric ozone levels and potentially triggering surface ozone pollution events [19–23].

In recent years, ozone pollution in China has been continuously aggravated, with concentrations and exceedance frequencies being significantly elevated [24–26]. Enhanced anthropogenic emissions have been identified as one of the primary drivers of worsening ozone pollution in economically developed regions [27,28]. Compared to plains, plateaus experience shorter vertical transport distances of stratospheric air masses to the surface. Consequently, the role of vertical transport in enhancing surface ozone levels requires prioritized consideration. Although numerical simulations indicate that stratospheric ozone accounts for only 5–10% of tropospheric ozone, the downward transport of stratospheric ozone can lead to significant increases in surface ozone concentrations [29]. Using an atmospheric chemical transport model, Zhang et al. [30] found that during a summer 2019 ozone pollution episode in north China, stratospheric intrusions contributed 6–20% to near-surface ozone. A short-term increase of 40–50 ppbv in surface ozone concentrations caused by stratospheric intrusions was also observed in 2021 [31]. Current research over the Tibetan Plateau has primarily focused on the spatial distribution characteristics and dynamical mechanisms of total atmospheric ozone columns [32,33] or spatiotemporal variations in surface ozone at representative urban and background sites (including Lhasa, Nam Co Lake, and Waliguan Baseline Observatory) [34–36]. Research on stratospheric intrusion (SI) over the Tibetan Plateau has not been sufficiently explored in terms of characterizing its temporal evolution patterns. The mechanisms by which SI influences surface-level ozone remain unclear, and there is still significant uncertainty regarding its proportional contribution.

This study examines the ozone variation patterns in Xining (a city on the northeastern Tibetan Plateau) using ground observations, reanalysis data, and an algorithm for stratospheric intrusion events, and it quantifies the long-term influence of stratospheric intrusions on surface ozone. Additionally, by analyzing a typical ozone pollution episode, it explores the formation mechanisms of ozone pollution, particularly the role of stratospheric vertical transport. The results could provide both scientific evidence and practical references for regional ozone assessment and pollution control strategies in plateau regions.

2. Materials and Methods

2.1. Observational and Reanalysis Data

Study area: Xining (36.57° N, 101.82° E) is a high-altitude city situated in the northeastern Tibetan Plateau, with a mean elevation of 2261 m above sea level and a 2024 resident population of 2.48 million. The region exhibits comparatively low anthropogenic pressure and industrial emissions.

Ground observational data: Hourly concentrations of surface ozone (O_3) and carbon monoxide (CO) were obtained from 5 sites in Xining from the National Urban Air Quality Real-time Publishing Platform provided by the Ministry of Ecology and Environment (MEE) of China (Figure 1). In the study, a fully automatic z-score-based outlier detection method for data quality control was implemented [37,38]. Outliers caused by instrument malfunctions and measurement errors were removed to ensure data validity. According to the technical regulation for ambient air quality assessment of China (HJ 663-2013) [39], the maximum daily 8 h average ozone concentration (MDA8 O_3) was calculated as the evaluation metric for daily ozone levels. The statistical results were considered valid when at least fourteen 8 h moving average values were available between 08:00 and 24:00 local time.

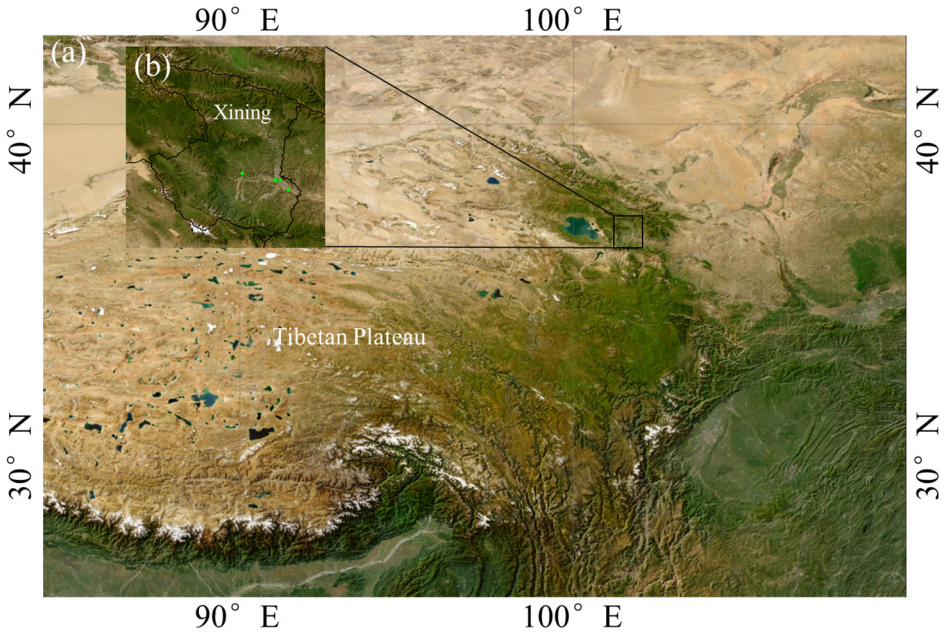


Figure 1. Topographic map and distribution of surface monitoring sites of the study area. (**a**) Topographic map of Xining and its surrounding area; (**b**) surface monitoring sites (green dots) in Xining.

Reanalysis data: Meteorological parameters were extracted from the fifth-generation European Centre for Medium-Range Weather Forecasts (ECMWF) atmospheric reanalysis of the global climate (ERA5) (0.25° × 0.25° spatial resolution). Surface variables, including 2 m temperature, 2 m dew point temperature, 10 m wind speed/direction, and ultraviolet radiation, were obtained at hourly intervals. Vertical profile data, including geopotential height (700/500 hPa), ozone concentration, vertical velocity, potential vorticity, temperature, and dew point temperature, were acquired at a 6 h resolution. These datasets were used in the comprehensive analysis of synoptic patterns, local meteorological conditions, and transport mechanisms during pollution episodes.

2.2. Identification of Stratospheric Intrusion to Surface (SITS) Events

Chen et al. [40] developed a method for detecting prolonged stratospheric intrusion to surface (SITS) events based on high-spatiotemporal-resolution ground pollutant data (e.g., O_3 and CO). This approach considers the rich-O_3 and poor-CO properties of stratospheric air reaching the surface. It has been demonstrated to be effective for the rapid and direct detection of SI events [41–43]. In this study, aged stratospheric air that had reached the surface but lost its stratospheric characteristics was excluded [41].

Based on hourly measurements of surface O_3 and CO, we identified SITS events using the following criteria:

1. Event start

First, we calculated the hourly variations in O_3 and CO concentrations throughout the year. The 95th percentile of annual O_3 increase rates (O_3cr95%) and the 5th percentile of annual CO decrease rates (COcr5%) were selected to identify the sudden peaks that occur when stratospheric air initially reaches the surface. The time t is defined as the event start time when both of the following conditions were simultaneously satisfied: O_3cr(t) ≥ O3cr95% and COcr(t) ≤ COcr5%. The co-occurrence of extreme O_3 increases and extreme CO decreases helped distinguish between surface O_3 rapid enhancement caused by stratospheric intrusions and those resulting from O_3 horizontal regional transport or photochemical processes [44].

2. Event validation

During SITS events, surface O_3 concentrations are expected to increase significantly above background levels. To minimize interference from local photochemical production, we implemented two diagnostic thresholds:

(1) At SITS start hour, the O3 concentration should exceed the seasonal noontime average (O3noon-season) when photochemical reactions are relatively active.
(2) Throughout the SITS duration, CO levels must remain below their seasonal mean (CO-season).

3. Event termination

Due to the tropospheric mixing processes, the properties of the intruded stratospheric air subside over time. The SITS event was considered terminated when the O_3 concentration decreased to the seasonal average level (O_3-season) or the CO concentration exceeded the CO seasonal average (CO-season). Stratospheric and tropospheric air are indistinguishable.

2.3. Quantification of SITS Contributions to Surface Ozone

The contribution of SITS to surface ozone was estimated through a three-stage process.

1. Calculate seasonal hourly mean surface O_3 concentration

For each season over each year, the hourly average surface O_3 concentration is computed (denoted as $O_3^{h-season}$, where h = 1, 2, 3, . . ., 24). The O_3h-season values are taken as reference baselines to measure the departure of O_3 concentrations from their baselines during SITS periods.

2. Quantify stratospheric O_3 intrusion during SITS events

Based on the start and end times of the SITS event, the hourly O_3 concentrations exceeding $O_3^{h-season}$ during the SITS period are summed. This cumulative excess is defined as the stratospheric O_3 intruding into the surface layer O_3^{SITSin}:

$$O_3^{SITSin} = \int_{SITS_start}^{SITS_end} \left(O_3^h - O_3^{h-season} \right) dt \quad (1)$$

where O_3^h represents the hourly O_3 observations at hour h, and $O_3^{h-season}$ represents the baseline O_3 concentrations for the same hour. The differences $\left(O_3^h - O_3^{h-season}\right)$ are summed over the SITS period with a temporal resolution of 1 hour (i.e., dt = 1 h).

The total O_3 concentration over the SITS period (denoted as O_3^{SITS}) is computed simultaneously by summing all O_3 concentrations during each SITS event according to Equation (2):

$$O_3^{SITS} = \int_{SITS_start}^{SITS_end} O_3^h dt \quad (2)$$

3. Determine the contribution ratio (R_{SITS})

Finally, the contribution of the SITS event to surface O_3 is quantified as the following ratio:

$$R_{SITS} = \frac{O_3^{SITSin}}{O_3^{SITS}} \times 100\% \quad (3)$$

3. Results and Discussion

3.1. Characteristics of Surface Ozone in Xining

Monthly variations in the maximum daily 8 h average ozone (MDA8 O_3) in Xining (2019–2023) were analyzed. The average ozone concentration was recorded at 94 $\mu g/m^3$.

Ozone during the summer months in 2021–2023 (127 μg/m^3) showed a significant increase compared to 2019–2020 (118 μg/m^3). Annual average ozone exhibited a sustained upward trend from 2019 to 2022, followed by a decline in 2023 (Figure 2). Seasonal comparison demonstrated that the average summer ozone concentration reached 123 μg/m^3 over five years, with the highest level recorded in 2021 (129 μg/m^3). July exhibited the highest ozone in summer, followed by June and August. Monthly values exceeded 130 μg/m^3 in July 2021, June and July 2022, and July 2023. The average ozone in spring and autumn were 103 μg/m^3 and 85 μg/m^3, respectively. Monthly levels in April (102 μg/m^3), May (115 μg/m^3), and September (101 μg/m^3) exceeded 100 μg/m^3. The results showed that relatively high ozone levels in Xining were primarily concentrated in the warm season (April–September).

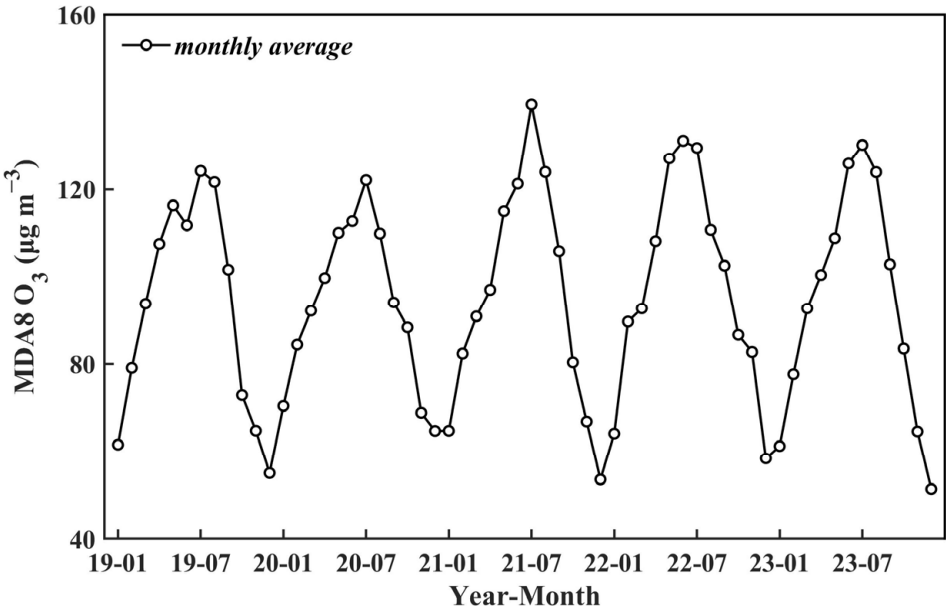


Figure 2. Monthly variation in MDA8 O_3 in Xining, 2019–2023.

To investigate the variation in ozone pollution in Xining, the ozone exceedance conditions from 2019 to 2023 were also analyzed. Using China's Ambient Air Quality Standards (GB 3095-2012) [45] Class II (160 μg/m^3) as the threshold, we identified 29 ozone exceedances days over five years, with 62% (18 days) concentrated in 2021, consistent with the maximum summer ozone in that year. Other years recorded fewer than seven annual exceedances. Subsequently, we observed a marked increase in potential ozone exceedance days when applying more stringent criteria (O_3 > 150 μg/m^3 and >140 μg/m^3). The number of days with ozone exceeding 140 μg/m^3 remained around 10 days annually in 2019 and 2020. Then, potential exceedance days showed notable growth in the subsequent three years. Excluding the anomalously high frequency observed in 2021, exceedance days in 2022–2023 exhibited significant increases in days above 150 μg/m^3 (from 5 days to >10 days) and in days above 140 μg/m^3 (from 12 to >18 days) compared to that in 2019–2020 (Table 1). The increase in potential pollution days implies a higher probability of air quality exceedance events in Xining.

Table 1. Mean concentration of MDA8 O_3 and number of exceeding days in Xining, 2019–2023.

Year		2019	2020	2021	2022	2023
Average concentration ($\mu g\ m^{-3}$)	All	92	93	95	99	94
	Spring	106	101	101	109	101
	Summer	120	115	129	124	127
	Autumn	80	84	86	90	84
	Winter	63	72	66	70	69
Number of days >X$\mu g\ m^{-3}$	>160	0	3	18	7	1
	>150	3	5	27	11	10
	>140	10	12	43	31	18

3.2. Characteristics and Contribution Assessment of SITS Events

To assess the impacts of vertical transport on local ozone, we analyzed the temporal variation patterns of stratospheric intrusion to surface (SITS) events in Xining from 2019 to 2023 and quantified their contributions to surface ozone. Based on the method described in Section 2.2 and ground gaseous pollutant observation data, we identified the SITS events that occurred between 2019–2023. Figure 3 displays the frequency and mean duration of the events. A total of 42 SITS events were detected in Xining from 2019 to 2023. The event duration was 8.4 h, which indicated that SITS could consistently affect surface ozone for at least 8 h on average. During the study period, spring exhibited the highest frequency and duration of SITS events among all seasons, which is consistent with previous climatological research [46,47]. There were 13 events recorded, with an average 10.1 h duration. April was observed to have the highest event frequency, with seven occurrences recorded at an average duration of 7.6 h. Although only four events were detected in May, their impact on surface conditions was found to be more prolonged, with durations reaching 15.8 h. A total of 11 events were found in both autumn and winter. The duration in autumn (7.7 h) was slightly longer than that in winter (7.1 h). October was observed to have a relatively longer duration in these two seasons, with 11.5 h on average. Summer exhibited the lowest event frequency (seven occurrences) but demonstrated a longer duration of 8.4 h compared to autumn and winter. This suggested that stratospheric intrusions during summer could still exert persistent effects on surface ozone. From June to August, event frequencies ranged between 2–3 occurrences per month. However, July showed significantly longer durations (10 h) compared to other months. As July was also the month with the highest ozone concentration, vertical transport was more likely to lead to ground-level pollution.

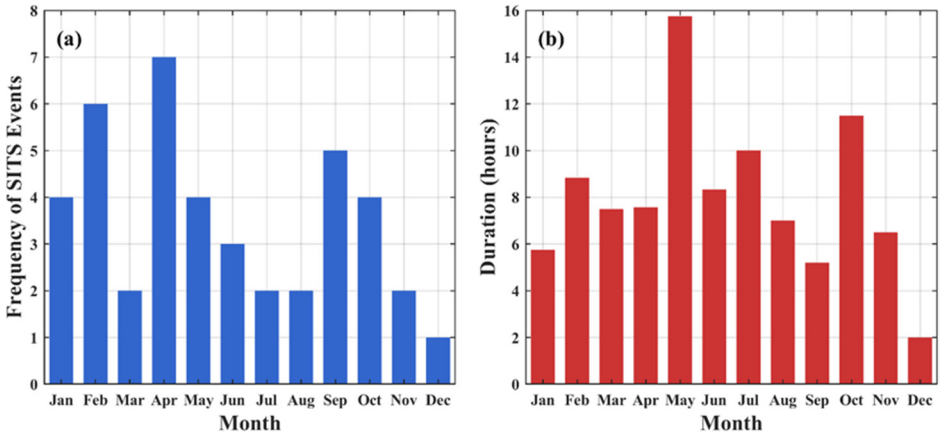


Figure 3. Frequency and average duration of SITS events in Xining, 2019–2023. (**a**) Frequency of SITS events; (**b**) average duration (hours) of SITS events.

Furthermore, by calculating the excess ozone concentration in SITS events relative to seasonal hourly averages, we estimated both the enhanced surface ozone concentrations (unit: μg/m^3/h) and contribution ratios from stratospheric ozone intrusions during these events. Figure 4 presents the monthly averaged ozone enhancement during SITS events. July exhibited significantly higher enhancement values (51.9 μg/m^3/h) compared to other months. The summertime elevation of the tropopause facilitates the downward transport of stratospheric air masses with higher origins in the stratosphere, which may carry more ozone into the troposphere [48,49]. Enhancements in most months ranged between 16–30 μg/m^3/h, while January, November, and December demonstrated weaker intrusion intensities (2.3–10.3 μg/m^3/h). As shown in Figure 4b, the stratospheric influence varied substantially across months. July and February had the highest contributions, exceeding 30%, while November showed the weakest contribution at only 2.7%. Contributions in spring and autumn months (except for November) ranged primarily between 14% and 25%. Collectively, SITS events contributed an average of 19.7% to ozone concentrations, indicating the substantial role of stratospheric intrusions in elevating near-surface ozone.

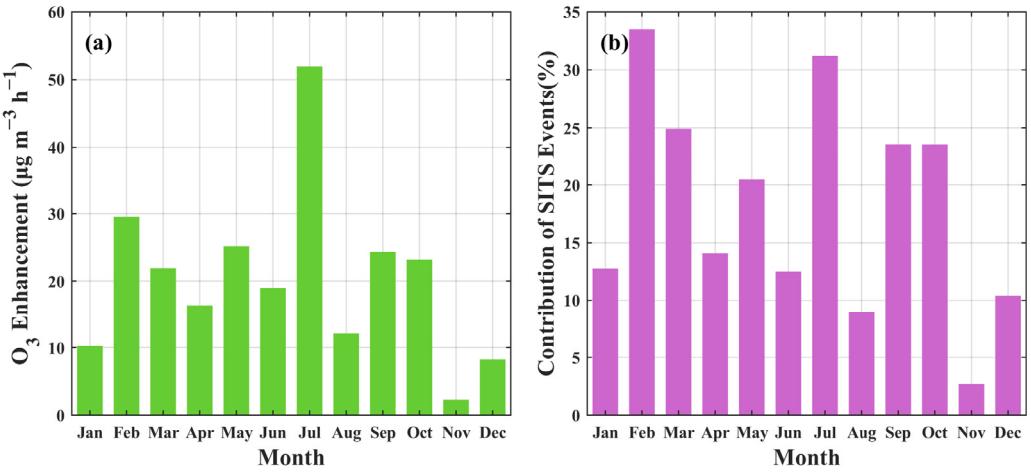


Figure 4. Enhanced concentrations and contribution to surface ozone of SITS events in Xining, 2019–2023. (**a**) Enhanced concentrations to surface ozone of SITS events; (**b**) contribution to surface ozone of SITS events.

Furthermore, the relationship between SITS events and ozone pollution was analyzed. An O_3 exceedance day is considered SITS-associated if the concentration exceeds the pollution threshold during a SITS event. Based on the three thresholds used in Section 3.1, Table 2 presents the number of O_3 exceedances in SITS events. Although SITS events in spring, autumn, and winter exhibited relatively high frequency and intensity, all event-related ozone concentrations were below the Chinese Class II standard (160 μg/m^3). Three exceedances were recorded in summer. This may be attributed to the comparatively lower background of O_3 in the Tibetan Plateau [50,51]. Under more stringent pollution thresholds, there were one and two ozone exceedance events (>150 and >140 μg/m^3) recorded in May, whereas the number in summer months (June, July, August) was significantly higher, with four (>150 μg/m^3) and 5 (>140 μg/m^3), constituting over 55% of the total SITS events. Therefore, SITS events in Xining from May to August not only increase regional ozone background levels but also likely to cause the occurrence of air pollution.

Table 2. Averaged surface O_3 concentrations in each month and the number of SITS events with O_3 exceedance under different standards from 2019–2023.

Month	Average Concentration ($\mu g\ m^{-3}$)	Number of O_3 Exceedance (>X $\mu g\ m^{-3}$) in SITS Events		
		>160	>150	>140
1	65	0	0	0
2	83	0	0	0
3	92	0	0	0
4	102	0	0	0
5	115	0	1	2
6	120	1	1	2
7	129	2	2	2
8	118	0	1	1
9	101	0	0	0
10	83	0	0	0
11	70	0	0	0
12	58	0	0	0

3.3. Stratospheric Intrusion Mechanisms in Ozone Pollution Formation

Previous analyses have revealed that during the study period, the highest ozone concentrations and pollution frequency in Xining were recorded in summer months, particularly in July. The maximum event intensity and stratospheric intrusion contributions were also found in this period. Consequently, this section focuses on a representative ozone pollution episode in July 2021, which coincided with a SITS event, to elucidate its formation mechanisms, especially the impact of stratospheric intrusion.

A severe ozone pollution episode occurred in Xining from 25 July to 3 August 2021. Both the duration and pollution intensity of this episode substantially exceeded historical averages, with the average concentration reaching 141 $\mu g/m^3$. The event showed 17.6% and 11.1% increases compared to the summer and the July average, respectively.

As shown in Figure 5, at the beginning of the episode (25 July 2021), all monitoring stations recorded concentrations below China's Ambient Air Quality Standards (GB 3095-2012) Class I (100 $\mu g/m^3$), with a city mean of 79 $\mu g/m^3$. Subsequently, ozone concentrations rose sharply above 100 $\mu g/m^3$ from 26 July (134 $\mu g/m^3$), with one monitoring station (20% of the total) exceeding 140 $\mu g/m^3$. On 29 July, the average concentration had risen to 154 $\mu g/m^3$, closely approaching but remaining below the Chinese Class II standard (160 $\mu g/m^3$). A total of 80% and 60% of the stations exceeded 140 $\mu g/m^3$ and 150 $\mu g/m^3$, respectively. During the peak phase (30 July–2 August) of the pollution episode, the regional ozone level reached 167 $\mu g/m^3$, 19.3% higher than the monthly average in July 2021. Notably, the daily maximum ozone occurred on 31 July (173 $\mu g/m^3$), with 60% of the stations (/three3 sites) above 170 $\mu g/m^3$. On 3 August, concentrations at more than 50% of the stations decreased below the Chinese Class I standard (100 $\mu g/m^3$). The mean ozone concentration dropped sharply from 160 $\mu g/m^3$ on 2 August to 99 $\mu g/m^3$, indicating the termination of this pollution episode.

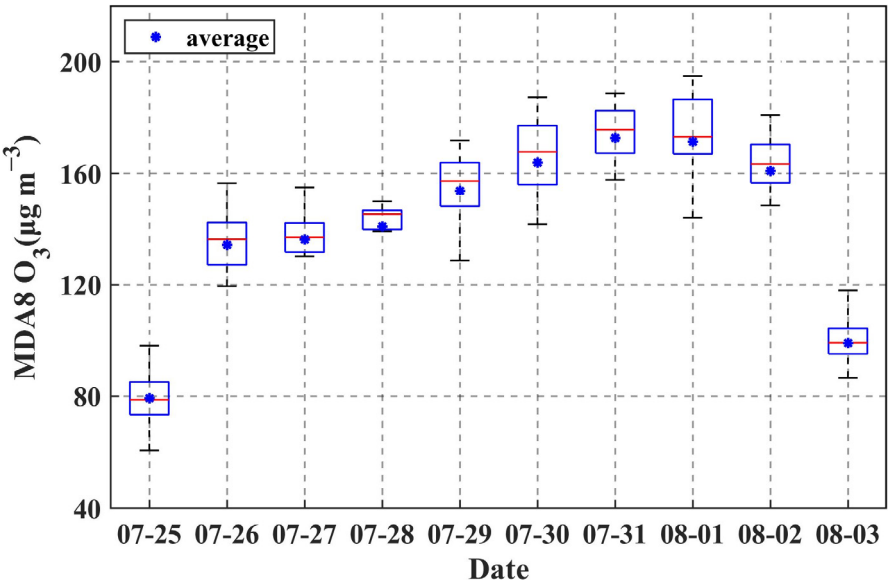


Figure 5. Daily variation in MDA8 O_3 in Xining from 25 July to 3 August 2021. In each boxchart, the blue dots represent the city averaged concentration, the red line is the median, the top and bottom are the maximum and minimum values, and the upper and lower blue boxes are the 75% and 25% quantiles.

The meteorological mechanisms of the pollution formation were analyzed. Figure 6 displays the circulation patterns and distribution characteristics of key meteorological factors during different phases of the episode in Xining. Due to the plateau location of the study area (altitude 2000–3000 m), we used the geopotential height field at 700 hPa to characterize the near-surface circulation conditions. On 25 July, flat northwest wind prevailed over the upper atmosphere in Xining. The surface was located at the leading edge of the high-pressure system, dominated by north wind. From 26 July to 29 July, the region was controlled by high-pressure or uniform pressure fields, exhibiting minimal sea-level pressure gradients. The surface layer displayed weak north winds. This resulted in progressive deterioration of atmospheric dispersion and a marked elevation in O_3 concentrations. As illustrated in Figure 7, the mean relative humidity declined from 80% to 52% on 29 July, while the average daily maximum temperature rose to 23.2 °C. These meteorological changes created more favorable photochemical conditions of ozoneproduction.

During the peak stage of the episode (30 July–2 August), the 500 hPa geopotential height field corresponded to a post-trough and pre-ridge synoptic configuration, where northwest wind prevailed in the upper troposphere accompanied by dominant subsidence motion. Surface conditions remained under the dominance of a high-pressure system. Influenced by weak north winds and subsiding airflows, the mean relative humidity (RH) dropped below 50%, and wind speeds were between 1.1 and 1.4 m/s. The synergistic effect of weak winds and subsidence severely suppressed dispersion capacity, resulting in ozone accumulation and thereby sustaining regional ozone pollution. In this phase, the average daily maximum temperature (26.6 °C) showed a significant increase compared to the initiation phase (19.4 °C), and the daily cumulative radiation rose to 3.29×10^6 J/m^2 on 31 July. Both the daily maximum temperature and cumulative radiation exceeded historical ozone pollution episode averages (24.8 °C and 3.16×10^6 J/m^2) for the same period. The results indicated that prolonged increases in both temperature and radiation substantially enhanced the photochemical ozone production efficiency. Combined with extremely unfavorable diffusion conditions, these factors collectively led to the occurrence of persistent pollution. From the evening of 2 August to 3 August, cold air intrusion

induced rapid pollution scavenging in the study area, with an abrupt wind surge and a steep temperature decline.

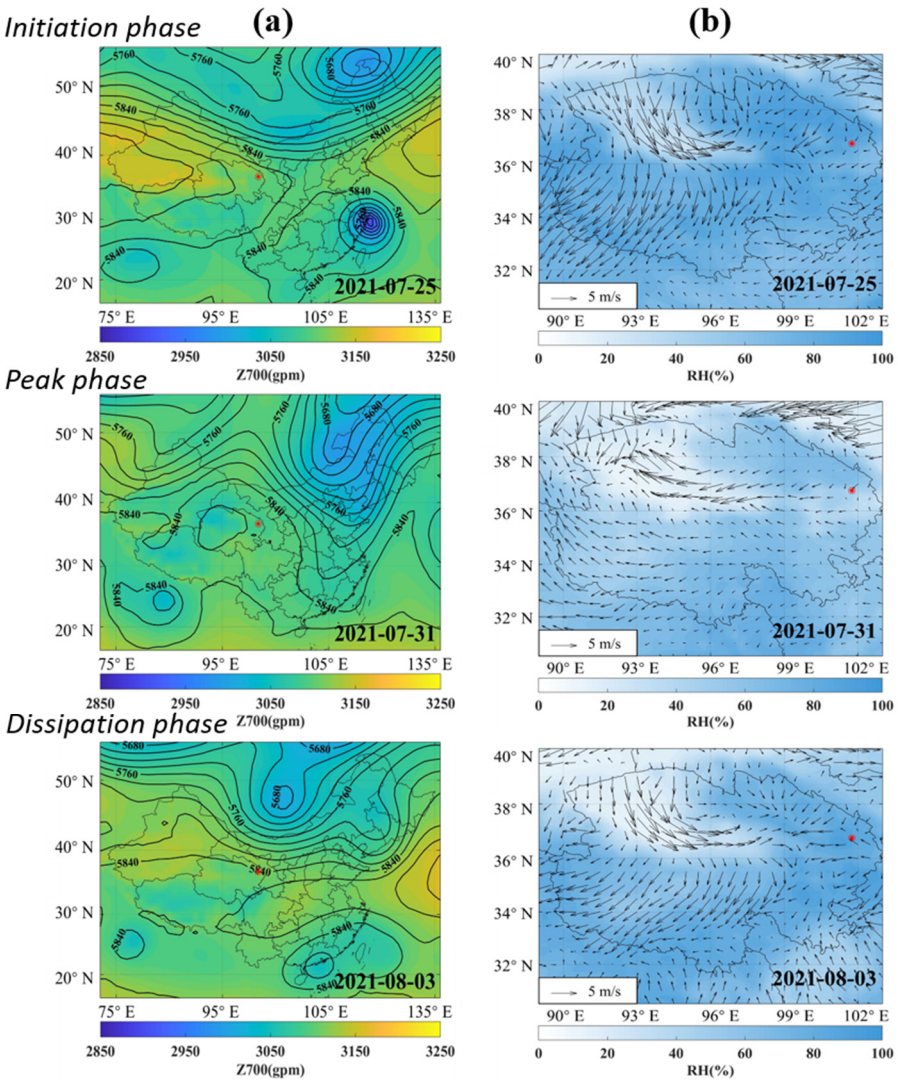


Figure 6. Composite distributions of meteorological factors in initiation phase, peak phase, and dissipation phase during the episode. (**a**) Geopotential height at 500 hPa (Z500) (contour; units: gpm) and geopotential height at 700 hPa (Z700) (shading; units: gpm); (**b**) 10 m wind fields (vectors) and surface RH (shading; units: %). Xining is marked by red dots.

Considering transport effects, Figure 6b shows weak regional wind speeds during the peak stage of the pollution episode, which revealed that no significant horizontal transport occurred in Xining and its surrounding area. Therefore, the subsequent analysis focuses on the role of vertical transport mechanisms during the episode.

The troposphere and stratosphere exhibit distinct dynamic and chemical characteristics, with marked distribution disparities in potential vorticity (PV), relative humidity, and ozone concentrations. Constituent exchange is commonly observed at the tropopause, mainly due to interactions between the stratosphere and troposphere. The potential vorticity (PV) of air masses is conserved in the absence of diabatic heating and frictional forcing. This feature allows PV to function as a dynamic tracer for atmospheric transport analysis [52,53]. Upper tropospheric PV values near the tropopause act as an indicator for identifying stratospheric intrusion that delivers ozone into the troposphere [54].

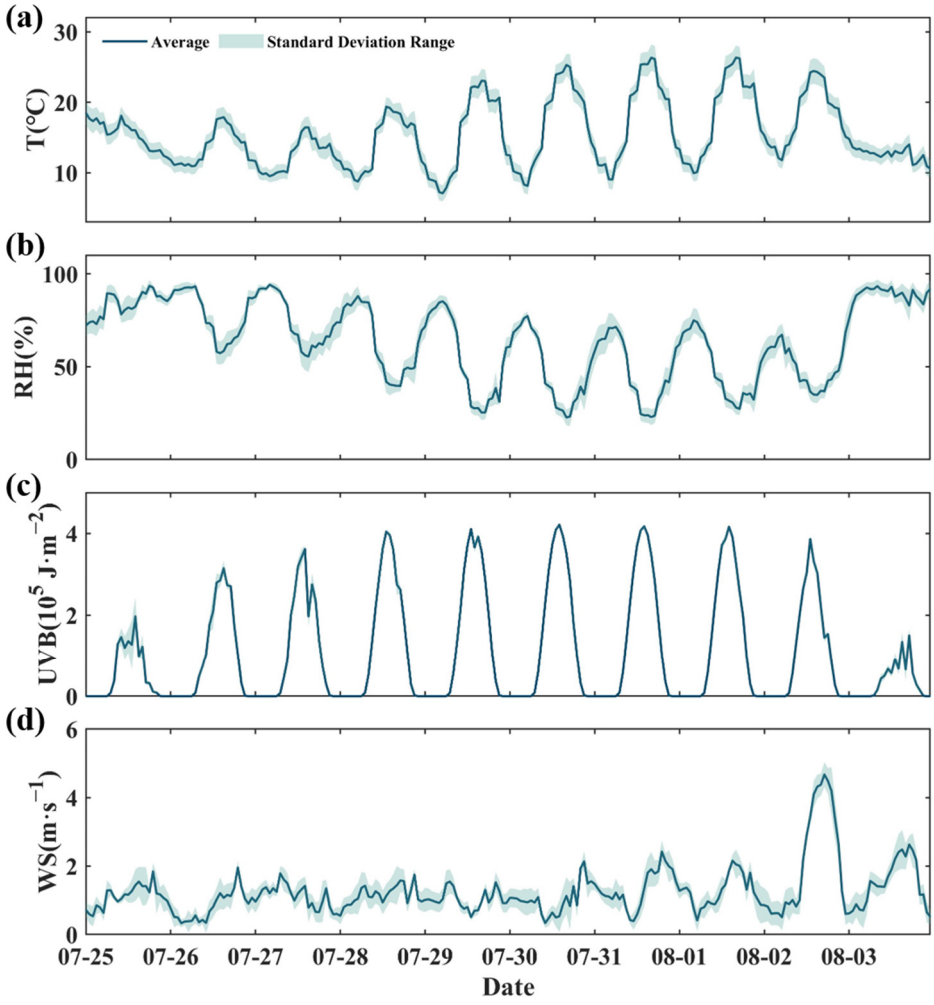


Figure 7. Time series of hourly meteorological factors of Xining from 25 July to 3 August 2021. (**a**) Temperature at 2 m (T) (units: °C); (**b**) surface relative humidity (RH) (units: %); (**c**) surface radiation (UVB) (units: 10^5 J m^{-2}); (**d**) wind speed at 10 m (WS) (units: m s^{-1}).

According to Figure 8, the vertical distribution of PV and tropospheric ozone concentrations exhibited a coherent evolution pattern during the study period. On 25 July, the 2 PVU (1 PVU = 10^{-6} K·m^2·kg^{-1}·s^{-1}) isoline was situated near the mean tropopause height (~15 km) without notable anomalies. High ozone distributions were primarily concentrated in the upper troposphere above 12 km. Vertical velocity profiles revealed strong upward motions in the mid-lower troposphere, accompanied by favorable near-surface dispersion conditions. The tropopause PV value increased to 3 PVU on 26 July, while the 2 PVU isoline descended to 12 km (200 hPa). From 27 July to 30 July, the PV at the tropopause remained persistently above 4 PVU, with the maximum value reaching 6 PVU. These PV anomalies provided direct evidence of stratosphere-to-troposphere transport, and the ozone concentration clearly showed a distinct increase in the mid-upper troposphere from its vertical distribution. The 2 PVU potential vorticity isoline was observed to descend markedly during 27–28 July, with its lowest elevation at 7 km (400 hPa), and stratospheric ozone-enriched air masses were transported into the mid-troposphere. Subsequently, as the upper-level folding intensity was enhanced, the spatial influence of these ozone-rich air masses was progressively expanded, accompanied by gradual ozone concentration increases being recorded in the mid-lower troposphere. A prominent high-O_3 zone was identified at 6–8 km (Figure 8a,b). Driven by intense subsidence flow at the mid-lower troposphere, the high-O_3 zone penetrated to the near-surface area (3 km) on 29 July (Figure 8a,c). According

to the method described in Section 2.2, a SITS event was simultaneously detected, further confirming that stratospheric ozone had been transported to the ground. The estimation results revealed that stratospheric intrusion contributed 24% to the surface ozone concentration. Notably, if the influence of stratospheric input was excluded, the ozone would likely not have exceeded 160 μg/m^3. This demonstrated that vertical transport was a critical driving mechanism in this pollution episode.

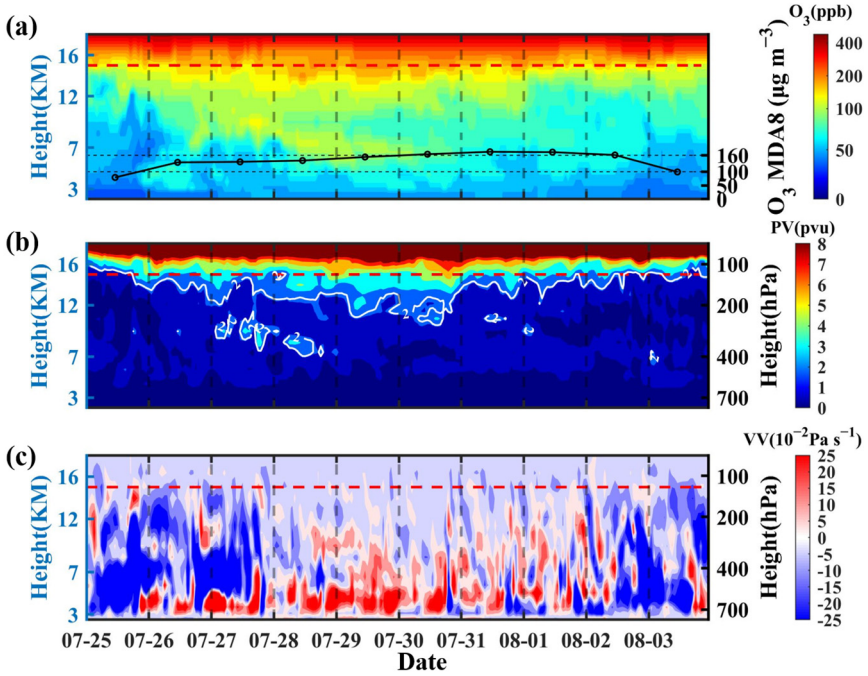


Figure 8. Time series of vertical profiles of ozone, potential vorticity, and vertical velocity over the study area (91° E, 29.7° N). (**a**) Vertical ozone profile (color shading) with surface MDA8 O_3 (black line); (**b**) vertical potential vorticity profile (color shading) with the 2 PVU contour line (white contours); (**c**) vertical velocity profile (color shading, where red and blue represent downward wind and upward wind). The red dashed line indicates the climatological summer tropopause height over Xining.

The 2 PVU isoline gradually retreated to the mid-upper troposphere after 1st August, with a decline in ozone throughout the troposphere. However, due to cumulative effects from earlier stages and persistently unfavorable dispersion conditions, surface ozone persistently exceeded the Chinese Class II standard (Figure 8a,c). On 3 August, strong upward motion developed in the mid-lower troposphere, and a low-ozone zone formed over the region. With no vertical input and combined with effective atmospheric dispersion, the surface pollution episode ended.

4. Conclusions

Based on observation and reanalysis data, this study revealed the characteristics of surface ozone evolution in Xining, a city on the northeastern Tibetan Plateau, in recent years. From 2019 to 2023, ozone concentrations in Xining exhibited a fluctuating upward trend, with an average maximum daily 8 h average (MDA8 O_3) of 94 μg/m^3. The high ozone values were predominantly concentrated in summer (123 μg/m^3), especially in July. During the study period, there were 29 days exceeding the Chinese secondary air quality standard (160 μg/m^3), with the highest frequency occurring in 2021. Notably, under stricter thresholds, the number of potential exceedance days (MDA8 O_3 > 150 μg/m^3 and >140 μg/m^3) showed a significant increasing trend from 2022 to 2023.

To further analyze the long-term impacts of stratospheric intrusion on regional ozone, high-resolution ground environmental data were utilized to identify stratospheric intrusion to surface (SITS) events. From 2019 to 2023, a total of 42 SITS events were identified, with an average duration of 8.4 h, and the highest frequency of events occurred in spring. Meanwhile, the contribution of SITS events to surface ozone was quantified. Over the five-year period, the average contribution rate of stratospheric intrusion was 19.7%. Overall, the highest hourly enhancement concentrations and contribution rate were both observed in July.

A comprehensive analysis was conducted on the evolution and formation mechanisms of a typical ozone pollution episode in Xining from 25 July to 3 August 2021. During the episode, intense warming, strong radiation, and low humidity significantly enhanced the photochemical reaction rates of ozone production. Under the combined effects of unfavorable dispersion conditions, ozone concentrations showed a marked increase. Anomalous dynamical structures were found in the troposphere over the region. The downward intrusion of the 2 PVU potential vorticity isoline into the mid-troposphere facilitated the transport of ozone-rich stratospheric air masses toward the troposphere. These air masses were further driven to the ground by sustained subsidence, contributing approximately 24% to surface ozone concentrations. This vertical transport mechanism served as a critical driver of both ozone exceedances and the persistence of the pollution episode.

In summary, this study quantitatively assessed the impact of stratospheric intrusion on surface ozone in Xining using ground environmental data. Case studies demonstrated that in high-altitude, low-emission regions like the Tibetan Plateau, high ozone or exceedance events are closely linked to stratospheric transport. In summer, the elevated tropopause height may allow stratospheric intrusions to deliver ozone with higher concentrations, significantly amplifying surface ozone. Combined with active local photochemical processes, this creates a synergistic amplification effect, exacerbating regional pollution risks. Future research could focus on long-term variations in stratosphere–troposphere exchange (STE) processes and their potential modulation under climate change, which could provide a theoretical foundation for ecological conservation and air quality management on the Tibetan Plateau.

Author Contributions: Conceptualization, M.L. and L.C.; methodology, M.L.; software, M.L. and Y.K.; validation, M.L. and Y.K.; formal analysis, M.L.; investigation, M.L. and M.F.; resources, C.Y. and Y.Z.; data curation, M.L. and J.G.; writing—original draft preparation, M.L.; writing—review and editing, M.L., J.T., and L.C.; visualization, M.L.; supervision, L.C.; project administration, M.L.; funding acquisition, J.T. All authors have read and agreed to the published version of the manuscript.

Funding: This research was funded by the National Key Research and Development Program of China (grant no. 2023YFB3907701), National Natural Science Foundation of China (grant no. 42171393), and Key Technology Research and Development Program in Priority Areas of Xinjiang Production and Construction Corps (grant no. 2024AB076).

Institutional Review Board Statement: Not applicable.

Informed Consent Statement: Not applicable.

Data Availability Statement: The raw data supporting the conclusions of this article will be made available by the authors on request.

Conflicts of Interest: The authors declare no conflicts of interest.

References

1. Avnery, S.; Mauzerall, D.L.; Liu, J.F.; Horowitz, L.W. Global crop yield reductions due to surface ozone exposure: 1. Year 2000 crop production losses and economic damage. *Atmos. Environ.* **2011**, *45*, 2284–2296. [CrossRef]
2. Sicard, P.; Anav, A.; De Marco, A.; Paoletti, E. Projected global ground-level ozone impacts on vegetation under different emission and climate scenarios. *Atmos. Chem. Phys.* **2017**, *17*, 12177–12196. [CrossRef]
3. Bell, M.L.; Goldberg, R.; Hogrefe, C.; Kinney, P.L.; Knowlton, K.; Lynn, B.; Rosenthal, J.; Rosenzweig, C.; Patz, J.A. Climate change, ambient ozone, and health in 50 US cities. *Clim. Change* **2007**, *82*, 61–76. [CrossRef]
4. Donzelli, G.; Suarez-Varela, M.M. Tropospheric Ozone: A Critical Review of the Literature on Emissions, Exposure, and Health Effects. *Atmosphere* **2024**, *15*, 779. [CrossRef]
5. Cui, Y.; Wang, J.; Wang, J.; Kang, M.; Zhao, H. Quantifying the Impact of Surface Ozone on Human Health and Crop Yields in China. *Atmosphere* **2025**, *16*, 162. [CrossRef]
6. Gong, C.; Liao, H.; Yue, X.; Ma, Y.; Lei, Y. Impacts of Ozone-Vegetation Interactions on Ozone Pollution Episodes in North China and the Yangtze River Delta. *Geophys. Res. Lett.* **2021**, *48*, e2021GL093814. [CrossRef]
7. Jacob, D.J.; Winner, D.A. Effect of climate change on air quality. *Atmos. Environ.* **2009**, *43*, 51–63. [CrossRef]
8. Utembe, S.; Rayner, P.; Silver, J.; Guérette, E.-A.; Fisher, J.; Emmerson, K.; Cope, M.; Paton-Walsh, C.; Griffiths, A.; Duc, H. Hot Summers: Effect of Extreme Temperatures on Ozone in Sydney, Australia. *Atmosphere* **2018**, *9*, 466. [CrossRef]
9. Fix, M.J.; Cooley, D.; Hodzic, A.; Gilleland, E.; Russell, B.T.; Porter, W.C.; Pfister, G.G. Observed and predicted sensitivities of extreme surface ozone to meteorological drivers in three US cities. *Atmos. Environ.* **2018**, *176*, 292–300. [CrossRef]
10. Jeong, J.I.; Park, R.J. Effects of the meteorological variability on regional air quality in East Asia. *Atmos. Environ.* **2013**, *69*, 46–55. [CrossRef]
11. Kou, W.; Gao, Y.; Zhang, S.; Cai, W.; Geng, G.; Davis, S.J.; Wang, H.; Guo, X.; Cheng, W.; Zeng, X.; et al. High downward surface solar radiation conducive to ozone pollution more frequent under global warming. *Sci. Bull.* **2023**, *68*, 388–392. [CrossRef] [PubMed]
12. Peralta, A.H.D.; Gavidia-Calderon, M.; Andrade, M.D.F. Future Ozone Levels Responses to Changes in Meteorological Conditions under RCP 4.5 and RCP 8.5 Scenarios over Sao Paulo, Brazil. *Atmosphere* **2023**, *14*, 626. [CrossRef]
13. Gong, C.; Lei, Y.; Ma, Y.; Yue, X.; Liao, H. Ozone–vegetation feedback through dry deposition and isoprene emissions in a global chemistry–carbon–climate model. *Atmos. Chem. Phys.* **2020**, *20*, 3841–3857. [CrossRef]
14. Kavassalis, S.C.; Murphy, J.G. Understanding ozone-meteorology correlations: A role for dry deposition. *Geophys. Res. Lett.* **2017**, *44*, 2922–2931. [CrossRef]
15. Wang, L.; Li, M.; Wang, Q.; Li, Y.; Xin, J.; Tang, X.; Du, W.; Song, T.; Li, T.; Sun, Y.; et al. Air stagnation in China: Spatiotemporal variability and differing impact on $PM_{2.5}$ and O_3 during 2013–2018. *Sci. Total Environ.* **2022**, *819*, 152778. [CrossRef]
16. Zhou, D.; Ding, A.; Mao, H.; Fu, C.; Wang, T.; Chan, L.Y.; Ding, K.; Zhang, Y.; Liu, J.; Lu, A.; et al. Impacts of the East Asian monsoon on lower tropospheric ozone over coastal South China. *Environ. Res. Lett.* **2013**, *8*, 044011. [CrossRef]
17. Liao, Z.; Gao, M.; Sun, J.; Fan, S. The impact of synoptic circulation on air quality and pollution-related human health in the Yangtze River Delta region. *Sci. Total Environ.* **2017**, *607–608*, 838–846. [CrossRef]
18. Zhang, X.; Zhou, L.; Zhang, X.; Luo, Y.; Sun, L. A Case Study on the Impact of East Asian Summer Monsoon on Surface O_3 in China. *Atmosphere* **2023**, *14*, 768. [CrossRef]
19. Ni, R.; Lin, J.; Yan, Y.; Lin, W. Foreign and domestic contributions to springtime ozone over China. *Atmos. Chem. Phys.* **2018**, *18*, 11447–11469. [CrossRef]
20. Lin, M.; Fiore, A.M.; Cooper, O.R.; Horowitz, L.W.; Langford, A.O.; Levy, H.; Johnson, B.J.; Naik, V.; Oltmans, S.J.; Senff, C.J. Springtime high surface ozone events over the western United States: Quantifying the role of stratospheric intrusions. *J. Geophys. Res. Atmos.* **2012**, *117*, D00V22. [CrossRef]
21. Li, D.; Vogel, B.; Müller, R.; Bian, J.; Günther, G.; Li, Q.; Zhang, J.; Bai, Z.; Vömel, H.; Riese, M. High tropospheric ozone in Lhasa within the Asian summer monsoon anticyclone in 2013: Influence of convective transport and stratospheric intrusions. *Atmos. Chem. Phys.* **2018**, *18*, 17979–17994. [CrossRef]
22. Chou, Y.; Huang, Q.; Zhang, Y.; Luo, J.; Wang, M.; Liao, H.; Zhang, Y.; Bai, Z. Impacts of deep boundary layer on near-surface ozone concentration over the Tibetan Plateau. *Atmos. Environ.* **2023**, *294*, 119532. [CrossRef]
23. Zhang, Y.; Zhao, T.; Ning, G.; Xu, X.; Chen, Z.; Jia, M.; Sun, X.; Shu, Z.; Lu, Z.; Liu, J.; et al. A Unique Mechanism of Ozone Surges Jointly Triggered by Deep Stratospheric Intrusions and the Tibetan Plateau Topographic Forcing. *Geophys. Res. Lett.* **2025**, *52*, e2024GL114207. [CrossRef]
24. Li, K.; Jacob, D.J.; Shen, L.; Lu, X.; De Smedt, I.; Liao, H. Increases in surface ozone pollution in China from 2013 to 2019: Anthropogenic and meteorological influences. *Atmos. Chem. Phys.* **2020**, *20*, 11423–11433. [CrossRef]
25. Wang, Y.; Gao, W.; Wang, S.; Song, T.; Gong, Z.; Ji, D.; Wang, L.; Liu, Z.; Tang, G.; Huo, Y.; et al. Contrasting trends of $PM_{2.5}$ and surface ozone concentrations in China from 2013 to 2017. *Natl. Sci. Rev.* **2020**, *7*, 1331–1339. [CrossRef]

26. Li, Y.; Zhang, Z.; Xing, Y. Long-Term Change Analysis of $PM_{2.5}$ and Ozone Pollution in China's Most Polluted Region during 2015–2020. *Atmosphere* **2022**, *13*, 104. [CrossRef]
27. Li, K.; Jacob, D.J.; Liao, H.; Shen, L.; Zhang, Q.; Bates, K.H. Anthropogenic drivers of 2013–2017 trends in summer surface ozone in China. *Proc. Natl. Acad. Sci. USA* **2019**, *116*, 422–427. [CrossRef] [PubMed]
28. Vazquez Santiago, J.; Hata, H.; Martinez-Noriega, E.J.; Inoue, K. Ozone trends and their sensitivity in global megacities under the warming climate. *Nat. Commun.* **2024**, *15*, 10236. [CrossRef]
29. Stevenson, D.S.; Dentener, F.J.; Schultz, M.G.; Ellingsen, K.; van Noije, T.P.C.; Wild, O.; Zeng, G.; Amann, M.; Atherton, C.S.; Bell, N.; et al. Multimodel ensemble simulations of present-day and near-future tropospheric ozone. *J. Geophys. Res. Atmos.* **2006**, *111*, 301. [CrossRef]
30. Zhang, Y.; Li, J.; Yang, W.; Du, H.; Tang, X.; Ye, Q.; Wang, Z.; Sun, Y.; Pan, X.; Zhu, L.; et al. Influences of stratospheric intrusions to high summer surface ozone over a heavily industrialized region in northern China. *Environ. Res. Lett.* **2022**, *17*, 094023. [CrossRef]
31. Chen, Z.; Liu, J.; Qie, X.; Cheng, X.; Shen, Y.; Yang, M.; Jiang, R.; Liu, X. Transport of substantial stratospheric ozone to the surface by a dying typhoon and shallow convection. *Atmos. Chem. Phys.* **2022**, *22*, 8221–8240. [CrossRef]
32. Sun, Y.; Zheng, X.; Bian, J.; Zhang, J.; Bai, Z. Vertical distribution of summer tropospheric ozone over the northern Tibetan Plateau. *Acta Meteorol. Sin.* **2022**, *80*, 806–818. [CrossRef]
33. Tobo, Y.; Iwasaka, Y.; Zhang, D.; Shi, G.; Kim, Y.S.; Tamura, K.; Ohashi, T. Summertime "ozone valley" over the Tibetan Plateau derived from ozonesondes and EP/TOMS data. *Geophys. Res. Lett.* **2008**, *35*, L16801. [CrossRef]
34. Yin, X.; Kang, S.; de Foy, B.; Cong, Z.; Luo, J.; Zhang, L.; Ma, Y.; Zhang, G.; Rupakheti, D.; Zhang, Q. Surface ozone at Nam Co in the inland Tibetan Plateau: Variation, synthesis comparison and regional representativeness. *Atmos. Chem. Phys.* **2017**, *17*, 11293–11311. [CrossRef]
35. Yin, X.; Kang, S.; Foy, B.d.; Rupakheti, D.; Rupakheti, M.; Cong, Z.; Wan, X.; Zhang, G.; Zhang, Q. Impacts of Indian summer monsoon and stratospheric intrusion on air pollutants in the inland Tibetan Plateau. *Geosci. Front.* **2021**, *12*, 101255. [CrossRef]
36. Zhang, Y.; Jin, J.-L.; Yan, P.; Tang, J.; Fang, S.-X.; Lin, W.-L.; Lou, M.-Y.; Liang, M.; Zhou, Q.; Jing, J.-S.; et al. Long-term variations of major atmospheric compositions observed at the background stations in three key areas of China. *Adv. Clim. Change Res.* **2020**, *11*, 370–380. [CrossRef]
37. Barrero, M.A.; Orza, J.A.; Cabello, M.; Canton, L. Categorisation of air quality monitoring stations by evaluation of PM_{10} variability. *Sci. Total Environ.* **2015**, *524–525*, 225–236. [CrossRef]
38. Song, C.; Wu, L.; Xie, Y.; He, J.; Chen, X.; Wang, T.; Lin, Y.; Jin, T.; Wang, A.; Liu, Y.; et al. Air pollution in China: Status and spatiotemporal variations. *Environ. Pollut.* **2017**, *227*, 334–347. [CrossRef]
39. *HJ 663–2013*; Technical Regulation for Ambient Air Quality Assessment. Ministry of Environmental Protection of China: Beijing, China, 2013.
40. Chen, Z.; Liu, J.; Qie, X.; Cheng, X.; Yang, M.; Shu, L.; Zang, Z. Stratospheric influence on surface ozone pollution in China. *Nat. Commun.* **2024**, *15*, 4064. [CrossRef]
41. Trickl, T.; Vogelmann, H.; Giehl, H.; Scheel, H.E.; Sprenger, M.; Stohl, A. How stratospheric are deep stratospheric intrusions? *Atmos. Chem. Phys.* **2014**, *14*, 9941–9961. [CrossRef]
42. Bartusek, S.; Wu, Y.; Ting, M.; Zheng, C.; Fiore, A.; Sprenger, M.; Flemming, J. Higher-Resolution Tropopause Folding Accounts for More Stratospheric Ozone Intrusions. *Geophys. Res. Lett.* **2023**, *50*, e2022GL101690. [CrossRef]
43. Langford, A.O.; Aikin, K.C.; Eubank, C.S.; Williams, E.J. Stratospheric contribution to high surface ozone in Colorado during springtime. *Geophys. Res. Lett.* **2009**, *36*, L12801. [CrossRef]
44. Granados-Muñoz, M.J.; Leblanc, T. Tropospheric ozone seasonal and long-term variability as seen by lidar and surface measurements at the JPL-Table Mountain Facility, California. *Atmos. Chem. Phys.* **2016**, *16*, 9299–9319. [CrossRef]
45. *GB 3095–2012*; Ambient Air Quality Standards. Ministry of Environmental Protection of China: Beijing, China, 2012.
46. Elbern, H.; Kowol, J.; Sládkovic, R.; Ebel, A. Deep stratospheric intrusions: A statistical assessment with model guided analyses. *Atmos. Environ.* **1997**, *31*, 3207–3226. [CrossRef]
47. Trickl, T.; Couret, C.; Ries, L.; Vogelmann, H. Zugspitze ozone 1970–2020: The role of stratosphere–troposphere transport. *Atmos. Chem. Phys.* **2023**, *23*, 8403–8427. [CrossRef]
48. Birner, T. Fine-scale structure of the extratropical tropopause region. *J. Geophys. Res. Atmos.* **2006**, *111*, D04104. [CrossRef]
49. Trickl, T.; Vogelmann, H.; Ries, L.; Sprenger, M. Very high stratospheric influence observed in the free troposphere over the northern Alps—Just a local phenomenon? *Atmos. Chem. Phys.* **2020**, *20*, 243–266. [CrossRef]
50. Liu, X.Y.; Yan, J.; Liu, H.; Niu, J.Q.; Yan, J.H.; Su, F.C. Spatial-temporal Variations and Driving Factors of Surface Ozone over the Qinghai-Xizang Plateau from 2015 to 2021. *Environ. Sci.* **2024**, *45*, 3778–3788. [CrossRef]
51. Lin, W.; Xu, X.; Zheng, X.; Dawa, J.; Baima, C.; Ma, J. Two-year measurements of surface ozone at Dangxiong, a remote highland site in the Tibetan Plateau. *J. Environ. Sci.* **2015**, *31*, 133–145. [CrossRef]
52. Hoskins, B.J.; McIntyre, M.E.; Robertson, A.W. On the Use And Significance of Isentropic Potential Vorticity Maps. *Q. J. R. Meteorol. Soc.* **1985**, *111*, 877–946. [CrossRef]

53. Appenzeller, C.; Holton, J.R.; Rosenlof, K.H. Seasonal variation of mass transport across the tropopause. *J. Geophys. Res.—Atmos.* **1996**, *101*, 15071–15078. [CrossRef]
54. Baray, J.L.; Ancellet, G.; Taupin, F.G.; Bessafi, M.; Baldy, S.; Keckhut, P. Subtropical tropopause break as a possible stratospheric source of ozone in the tropical troposphere. *J. Atmos. Sol.—Terr. Phys.* **1998**, *60*, 27–36. [CrossRef]

Disclaimer/Publisher's Note: The statements, opinions and data contained in all publications are solely those of the individual author(s) and contributor(s) and not of MDPI and/or the editor(s). MDPI and/or the editor(s) disclaim responsibility for any injury to people or property resulting from any ideas, methods, instructions or products referred to in the content.